RESEARCH ARTICLE

A Modified IRS Channel Model for MIMO Optical Wireless Communications with Geometric Constraints and Alignment Errors

Xin Zhong[1,*], **Zhihong Zeng**[2] **and Chen Chen**[2,*]

[1] Chongqing Electric Power College, Chongqing 400053, China
[2] School of Microelectronics and Communication Engineering, Chongqing University, Chongqing 400044, China

Abstract

Optical wireless communication (OWC) has emerged as a promising technology for high-speed indoor wireless access. Recently, mirror-based intelligent reflecting surface (IRS) has been introduced to OWC to enhance communication performance. However, traditional radio frequency IRS channel models fail to adapt optical features of OWC, and existing ideal optical models neglect some physical imperfections, leading to inaccurate performance evaluations in real-world deployments. To address this problem, this paper proposes a modified and more realistic IRS channel model. Distinct from ideal IRS channel, the proposed model employs a differential summation method to mathematically incorporate both geometric size constraints and random rotation angle errors of the IRS, thereby computing a more realistic IRS channel gain. Utilizing this modified channel model, we systematically evaluate and compare the relative communication performance under both single-input single-output (SISO) and multiple-input multiple-output (MIMO) systems. Simulation results demonstrate that IRS size variations and IRS rotation angle errors cause non-negligible negative impacts on MIMO-OWC systems, specifically leading to a loss in received optical power and a significant increase in inter-channel interference (ICI), thereby degrading overall system stability. In conclusion, the proposed modified channel model successfully demonstrates the realistic impacts and challenges of deploying IRS in practical OWC applications especially in MIMO setups. By capturing these results, this work provides a critical foundation and guidelines for the physical layout, hardware specifications, and robust beamforming design of future IRS-aided OWC systems.

Keywords: optical wireless communication, multiple-input multiple-output, intelligent reflecting surface, inter-channel interference.

Submitted: 26 May 2026
Revised: 22 June 2026
Accepted: 04 July 2026
Published: 08 August 2026

Vol. 1, **No.** 1, 2026.
10.62762/OWC.2026.926601

***Corresponding authors:**
Xin Zhong
zhongxin@cqepc.edu.cn
Chen Chen
c.chen@cqu.edu.cn

Citation
Zhong, X., Zeng, Z., & Chen, C. (2026). A Modified IRS Channel Model for MIMO Optical Wireless Communications with Geometric Constraints and Alignment Errors. *Optical Wireless Communication*, 1(1), 30–43.

1 Introduction

With the rapid proliferation of high-speed data services, the conventional radio frequency (RF) spectrum has become severely congested. As a result, OWC has emerged as an essential component of 6G systems [1], which is a wireless technology that transmits data via light waves. Typically, the transmitter employs a light-emitting diode (LED) or a laser diode (LD) to emit optical signals, which are subsequently captured by a photodetector (PD) at the receiver. Applications span the Internet of Things (IoT), vehicular networks, and UAV-based communication systems. Since light waves cannot penetrate obstacles and suffer from significant attenuation during transmission, OWC is highly dependent on the line-of-sight (LOS) channel. Consequently, link blockage can cause a devastating impact on OWC systems. Although non-line-of-sight (NLOS) channels provided by diffuse reflections offer some power compensation, the NLOS gain is too small to support high-speed transmission requirements [2]. Recently, intelligent reflecting surface (IRS) has emerged as a promising technology and a research hotspot in RF communications. An IRS consists of many reconfigurable reflecting elements, each capable of independently shifting the signal phase. By controlling these elements, the IRS enables directional signal reflection, directly optimizing the wireless communication link at the wireless channel [3]. Due to its advantages in channel control, IRS also exhibits excellent adaptability in OWC. Generally, two types of IRS are utilized in OWC: metasurface reflectors[4] and intelligent mirror reflectors[4]. Notably, mirror-based IRS is more widely utilized in OWC due to the excellent compatibility of its specular reflection mechanism with light waves. Compared to SISO systems, MIMO techniques offer significant advantages in OWC, such as substantially higher data rates and enhanced link reliability. However, the performance of MIMO-OWC systems is heavily dictated by the channel matrix, which is highly sensitive to the relative positioning of transmitters and receivers, leading to noticeable performance degradation in certain locations [5]. To mitigate this spatial vulnerability, the most common approach is to design an adaptive signal transmission scheme tailored to the specific channel characteristics [6]. However, relying solely on signal optimization may fall short in severe NLOS or blocked scenarios. To further overcome these limitations, multiple IRSs can be deployed to introduce additional optical links and fundamentally reconfigure the MIMO channel structure. By doing so, the system can adaptively fulfill the diverse requirements of various operational scenarios. Crucially, properly configuring these surfaces by establishing designated IRS-aided propagation paths between specific LEDs and PDs can optimize the channel characteristics and significantly enhance the overall system performance [7].

However, existing literature on IRS-aided MIMO-OWC systems predominantly focuses on algorithmic optimization, while the underlying channel models remain overly simplified. Classical models typically rely on an idealized point-to-point abstraction that assumes perfect alignment and neglects finite boundary constraints. In practical deployments, such simplifications fail to capture spatial errors and physical hardware boundaries. Specifically, due to the close proximity of multiple PDs in a MIMO setup, spatial tracking jitters cause the reflected beam footprint to shift and inevitably spill into adjacent non-intended PDs, inducing severe inter-channel interference (ICI). While this crosstalk is absent in single-PD links, it reshapes the MIMO channel matrix and drastically degrades the signal-to-noise ratio (SNR) and bit error rate (BER). To bridge these gaps, this paper proposes a high-fidelity modified IRS channel model and a precise computational approach to evaluate the realistic performance of mirror-based IRS in MIMO-OWC systems. The main contributions are summarized as follows:

- Proposal of a modified IRS channel model and a differential summation algorithm based on geometric optics and computational geometry to overcome the limitation of classical IRS channel model. Accurate calculation of the effective signal coverage and its overlap areas with different PDs by dividing the IRS into micro regions, which successfully shows the potential ICI in MIMO channel matrix.
- Evaluation of critical practical factors including IRS size, IRS rotational angle errors, and PD array spacing on system performance, which are factors that classical IRS channel models fail to consider.
- Comprehensive simulations under both SISO and MIMO scenarios to analyze IRS channel gains and BER performance, validating the accuracy and superiority of the proposed model over classical model.

The remainder of this paper is structured as follows: Section 2 reviews the related work to provide the necessary background for our study. Section 3 outlines the classical ideal IRS channel model, which serves as the baseline for our analysis. Building upon this, Section 4 establishes the modified IRS channel model. In Section 5, a differential summation algorithm tailored for the modified IRS channel gain is presented. Section 6 provides the simulation results and performance analysis, and Section 7 concludes the paper.

2 Related Work

IRS have emerged as a transformative technology in RF communications, enabling programmable signal reflection through an array of low-cost passive elements. Each element can independently adjust the phase shift of incident signals to achieve three-dimensional passive beamforming without requiring dedicated RF transmit chains [3]. This capability allows for dynamic control of wireless propagation environments, significantly enhancing link reliability and spectral efficiency in RF systems. However, the incoherent nature of OWC systems necessitates distinct IRS modeling approaches compared to RF counterparts. The fundamental channel characteristics of OWC, including the Lambertian radiation model and LOS/NLOS propagation properties, were established in early foundational work [8]. Building upon these foundations, it is first necessary to study the channel characteristics of the IRS in OWC. In [4], researchers derived the phase gradient for metasurface reflectors and the orientation mechanism for intelligent mirror reflectors to achieve precise directional reflection, validating their performance via simulations. Following this, in [9], researchers utilized radiometric concepts to investigate the channel characteristics of both metasurface and intelligent mirror reflector arrays in OWC. In [10], a comprehensive overview of the potentials and challenges of IRS-aided VLC was presented, further motivating research into more accurate channel modeling for practical deployments. Beyond indoor OWC, IRS-aided channel modeling has also been extended to free-space optical (FSO) communication systems [11], where the geometric analysis of mirror-based specular reflection similarly governs the channel gain computation, highlighting the broader applicability of reflection-based IRS models across different optical propagation scenarios. Subsequently, to enhance system performance, many studies have explored the application of IRS in OWC systems. In [12], researchers optimized the IRS configuration by maximizing the capacity of IRS-aided MIMO-OWC systems. Furthermore, in [13], researchers proposed a joint optimization of IRS configuration and transmit power to maximize the system capacity. Additionally, in [14], researchers focused on optimizing the IRS configuration by minimizing the mean square error (MSE) of the received signals in IRS-aided MIMO-OWC system.

In summary, while existing optimization frameworks have laid a solid foundation for IRS-OWC systems, they predominantly rely on idealized channel assumptions where physical geometric boundaries and alignment errors are entirely omitted. In contrast to these simplified studies, the core technical difference of our proposed model lies in breaking down the IRS into small regions and explicitly calculating the overlapping area between the reflected light and the PD boundaries. This approach provides a realistic baseline for evaluating actual system performance.

3 Classical Ideal IRS Channel Model

The widely adopted classical ideal mirror-based IRS channel model is illustrated in Figure 1, where P denotes an LED point source, M denotes one mirror of the IRS array, R denotes a PD, and S denotes the effective radiation area of P reflected by M. Consequently, its channel gain can be computed as[4]:

$$h_{\mathrm{IRS}}^{\mathrm{Cla}} = \begin{cases} \dfrac{l(m+1)\rho A}{2\pi(D_{\mathrm{M,P}}+D_{\mathrm{M,R}})^2}\cos^m(\varphi_{\mathrm{M,P}})T_s(\theta_{\mathrm{R,M}})\times \\ g(\theta_{\mathrm{R,M}})\cos(\theta_{\mathrm{R,M}}), \\ \qquad\qquad\qquad\qquad\qquad 0 \le \theta_{\mathrm{R,M}} \le \Phi \\ 0, \qquad\qquad\qquad\qquad\quad \theta_{\mathrm{R,M}} > \Phi \end{cases} \tag{1}$$

where $D_{\mathrm{M,P}}$ and $D_{\mathrm{M,R}}$ are the distance of P to the geometric center point of the M and the geometric center point of the M to R, respectively. $\varphi_{\mathrm{M,P}}$ is the emission angle between P and the geometric center point of M, and $\theta_{\mathrm{R,M}}$ is the incident angle between geometric center point of R and the geometric center point of M; $m = -\ln 2/\ln(\cos(\Psi))$ denotes the Lambertian emission order and Ψ is the semi-angle at half power of the LED; ρ and A are the responsivity and the active area of the PD, respectively; l is the reflectance coefficient of the IRS; $T_s(\theta_{\mathrm{R,M}})$ is the gain of the optical filter; $g(\theta_{\mathrm{R,M}}) = \frac{q^2}{\sin^2\Phi}$ is the gain of optical lens, where q and Φ are the refractive index and the half-angle field-of-view (FOV) of the optical lens, respectively. In fact, Eq.(1) is highly similar to the LOS channel gain because the indoor IRS channel satisfies the extremely near-field assumption[12]. Thus, the IRS channel can be regarded as an LOS channel that undergoes IRS reflection attenuation and extra

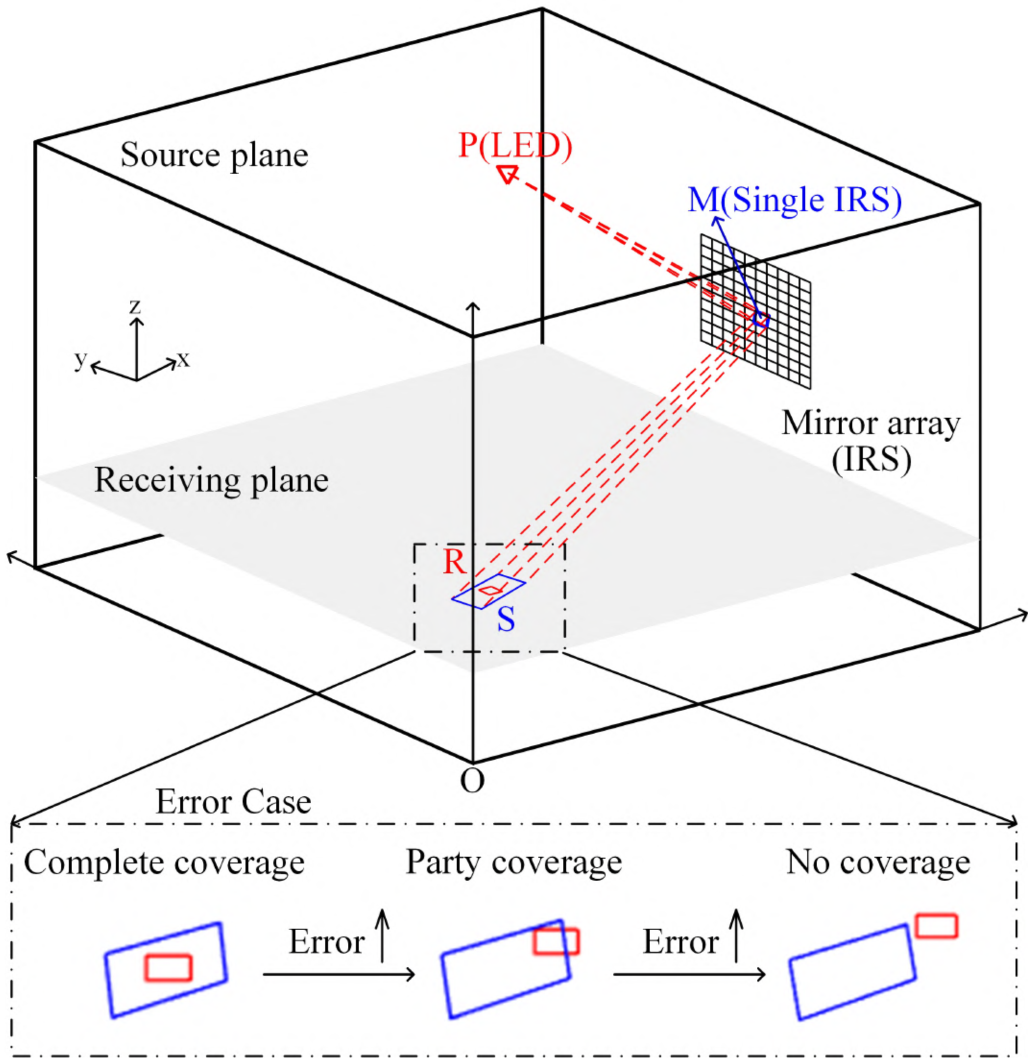

Figure 1. Classical ideal mirror-based IRS channel model.

propagation distance. Based on the analysis, Eq.(1) can be divided into two parts

$$E_{\mathrm{S}} = \frac{l(m+1)\cos^m(\varphi_{\mathrm{M,P}})}{2\pi(D_{\mathrm{M,P}}+D_{\mathrm{M,R}})^2}\cos(\theta_{\mathrm{R,M}}) \tag{2}$$

$$A_{\mathrm{E}} = \rho A T_s(\theta_{\mathrm{R,M}}) g(\theta_{\mathrm{R,M}}) \tag{3}$$

where E_{S} is the irradiance of S, and A_{E} is the photoelectric conversion coefficient over the entire PD surface[13]. Hence, establishment of Eq.(1) is based on the following conditions:

Point source assumption: The dimensions of the LED source P are considered negligible when compared with the distances between M and P. Hence, it allows us to deal with the LED source as a point.

Small reflector assumption: This assumption relies on the small area of the IRS M to ensure the consistency of the points M, i.e., $\varphi_{\mathrm{M,P}}$ and $\theta_{\mathrm{R,M}}$, which can be calculated using only the midpoint of M. Additionally, it ensures that the effective radiation area S has the same irradiance E_{S}.

Complete coverage: PD surface is fully encompassed by the effective radiation area S, guaranteeing that the entire PD area serves as an effective receiving area.

4 Modified IRS Channel Model

The classical IRS channel model is based on idealized assumptions. These simplifications ignore practical error scenarios. For example, IRS rotation angle errors can prevent the effective radiation area S from fully covering the receiver area R, leading to optical power loss. And increasing the IRS size to mitigate these angle errors would violate the small reflector assumption. More importantly, in MIMO-OWC systems, these practical errors also cause more interference issues, because reflected signals for

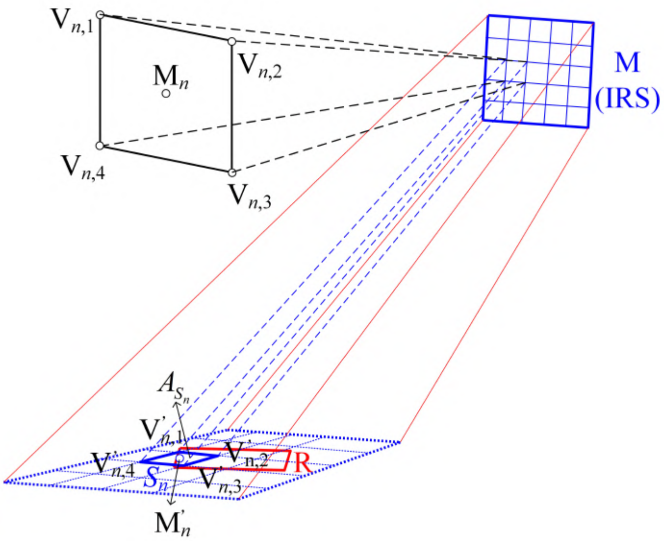

Figure 2. Schematic diagram of modified IRS channel.

one receiver may leak into adjacent receivers. Hence, ICI can change the channel matrix and influence the communication performance. Therefore, a modified IRS channel model is needed, which is introduced in this section.

4.1 Modified IRS Channel on SISO

To model potential ICI in MIMO-OWC systems, this section re-evaluates the IRS channel, starting with a SISO system. Eqs. (2) and (3) indicate that the IRS channel gain can be obtained as long as E_S and A_E are accurately calculated. To illustrate this, Figure 2 shows the schematic of the proposed modified IRS channel model. The modified model introduces a key structural improvement: a finite-sized IRS is discretized into N sufficiently small sub-IRSs. Physically, this discretization breaks the limitations of the classical point-to-point abstraction. By treating each tiny sub-IRS as a localized point source, every sub-IRS independently satisfies the standard geometric optics laws, thereby ensuring the strict validity of the small-reflector assumption across the entire surface. Take the n-th sub-IRS of reflector M as an example, its center point is $\mathrm{M_n}$, and its four vertices are denoted from $\mathrm{V_{n,1}}$ to $\mathrm{V_{n,4}}$. Based on specular reflection laws, we first locate the reflection point $\mathrm{M_n^{'}}$ of the light passing through $\mathrm{M_n}$ on the receiver plane. Using $\mathrm{M_n^{'}}$ as a reference, Eq. (2) yields the irradiance E_S of the effective coverage area $\mathrm{S_n}$ generated by this sub-IRS. Next, by tracking the reflection points $\mathrm{V_{n,1}^{'}}$ to $\mathrm{V_{n,4}^{'}}$ of the four vertices, the overlapping area between the effective coverage region $\mathrm{S_n}$ and the PD is determined. Then, the photoelectric conversion coefficient A_E of the PD is calculated via Eq.(3). Finally, the total IRS channel gain is obtained by summing the contributions of all sub-IRSs, which is expressed as follows:

$$h_{\mathrm{IRS}}^{\mathrm{Mod}} = \begin{cases} \sum\limits_{n=1}^{N} \dfrac{l(m+1)\rho A_{\mathrm{S}_n}}{2\pi(D_{\mathrm{M}_n,P}+D_{\mathrm{M}_n,\mathrm{M}_n'})^2}\cos^m(\varphi_{\mathrm{M}_n,P})\times \\ T_s(\theta_{\mathrm{M}_n,\mathrm{M}_n'})g(\theta_{\mathrm{M}_n,\mathrm{M}_n'})\cos(\theta_{\mathrm{M}_n,\mathrm{M}_n'}), \\ \qquad\qquad\qquad\qquad 0 \le \theta_{\mathrm{M}_n,\mathrm{M}_n'} \le \Phi \\ 0, \qquad\qquad\qquad\quad \theta_{\mathrm{M}_n,\mathrm{M}_n'} > \Phi \end{cases} \tag{4}$$

where A_{S_n} is the portion of the PD's active area illuminated by the n-th sub-IRS. Geometrically, as illustrated in Figure 2, $\Delta\mathrm{S}_n$ represents the irregular quadrilateral projected by the n-th sub-IRS onto the receiver plane, while ΔR represents the fixed physical boundary of the PD. A_{S_n} is the overlapping area between $\Delta\mathrm{R}$ and $\Delta\mathrm{S}_n$, which directly quantifies the exact portion of the reflected optical energy captured by the receiver and naturally encapsulates the alignment uncertainties. Hence, A_{S_n} can be expressed as:

$$A_{S_n} \triangleq \Delta S_n \cap \Delta\mathrm{R} \tag{5}$$

Obviously, $\Delta\mathrm{S}_n$ is defined as a closed quadrilateral formed by the four reflection points $\mathrm{V}_{n,1}^{'}$ to $\mathrm{V}_{n,4}^{'}$ on the receiver plane. And $\Delta\mathrm{R}$ is also defined by a closed quadrilateral. Based on this, A_{S_n} can be obtained by calculating the area of the polygon formed by the intersection of these two closed polygons. Computational geometry provides a mature and effective solution to this problem. First, the Greiner–Hormann algorithm [15] is used to find the intersection vertices of the two closed polygons. Then, a monotonic polygon triangulation algorithm [16] is applied to divide the intersecting polygon into several triangles. By summing the areas of all these triangles, A_{S_n} is determined.

4.2 Modified IRS Channel on MIMO

The greatest advantage of modified channel model is evident in MIMO systems. Typically, IRS are allocated to different sub-channels to meet specific requirements. This configuration may lead to potential channel interference. Specifically, the typical mathematical model of an IRS-aided MIMO system equipped with N_t LEDs and N_r PDs can be obtained by:

$$\mathbf{y} = \mathbf{H}\mathbf{x} + \mathbf{n}, \tag{7}$$

where $\mathbf{x} = [x_1, x_2, \cdots, x_{N_t}]^\mathrm{T}$ is the transmitted signal vector, $\mathbf{y} = [y_1, y_2, \cdots, y_{N_r}]^\mathrm{T}$ is the received signal vector, $\mathbf{n} = [n_1, n_2, \cdots, n_{N_r}]^\mathrm{T}$ denotes the additive white Gaussian noise vector, $\mathbf{n} \sim \mathcal{N}\left(0, \sigma_n^2\right)$.

$$\mathbf{H} = \mathbf{H}_{\mathbf{LOS}} + \mathbf{H}_{\mathbf{NLOS}} + \mathbf{H}_{\mathbf{IRS}} = \begin{bmatrix} h_{11,\mathrm{LOS}} & \cdots & h_{1N_t,\mathrm{LOS}} \\ \vdots & \ddots & \vdots \\ h_{N_r1,\mathrm{LOS}} & \cdots & h_{N_rN_t,\mathrm{LOS}} \end{bmatrix} + \begin{bmatrix} h_{11,\mathrm{NLOS}} & \cdots & h_{1N_t,\mathrm{NLOS}} \\ \vdots & \ddots & \vdots \\ h_{N_r1,\mathrm{NLOS}} & \cdots & h_{N_rN_t,\mathrm{NLOS}} \end{bmatrix} + \begin{bmatrix} h_{11,\mathrm{IRS}} & \cdots & h_{1N_t,\mathrm{IRS}} \\ \vdots & \ddots & \vdots \\ h_{N_r1,\mathrm{IRS}} & \cdots & h_{N_rN_t,\mathrm{IRS}} \end{bmatrix} \tag{6}$$

$\mathbf{H}$ represents the $N_r \times N_t$ MIMO channel matrix, which can be expressed as Eq.(6). Except for the IRS component, $\mathbf{H}_{\mathbf{LOS}}$ and $\mathbf{H}_{\mathbf{NLOS}}$ denote the LOS channel matrix and NLOS channel matrix, respectively, and their respective sub-channels $h_{rt,\mathrm{LOS}}$ and $h_{rt,\mathrm{NLOS}}$ between the t-th LED and the r-th PD can be expressed as [4]:

$$h_{rt,\mathrm{LOS}} = \begin{cases} \dfrac{(m+1)\rho A}{2\pi D_{r,t}^2}\cos^m(\varphi_{r,t})T_s(\theta_{r,t})\times \\ g(\theta_{r,t})\cos(\theta_{r,t}), & 0 \le \theta_{r,t} \le \Phi \\ 0, & \theta_{r,t} > \Phi \end{cases} \tag{8}$$

$$h_{rt,\mathrm{NLOS}} = \begin{cases} \displaystyle\sum_{w=1}^{W} \frac{(m+1)\rho A\varepsilon}{2(\pi D_{t,w}D_{r,w})^2}\cos^m(\varphi_{w,t})\cos(\alpha_{w,t}) \\ \times\cos(\beta_{r,w})T_s(\theta_{r,w})g(\theta_{r,w}) \\ \times\cos(\theta_{r,w})A_{\mathrm{wall}}, & 0 \le \theta_{r,w} \le \Phi \\ 0, & \theta_{r,w} > \Phi \end{cases} \tag{9}$$

For $\mathbf{H}_{\mathbf{IRS}}$, each sub-channel $h_{rt,\mathrm{IRS}}$ is the sum of gains provided by the IRS array between the t-th LED and r-th PD. However, due to ICI, these sub-channels contain both intended and unintended links. For instance, a reflection from LED 1 to PD 1 (intended for $h_{11,\mathrm{IRS}}$) may also illuminate PD 2, introducing unintended gain in $h_{21,\mathrm{IRS}}$. While the classical IRS channel model does not consider interference, the proposed modified IRS channel model captures it by calculating the overlap area between the IRS reflection area and all PDs. Consequently, this interference is directly integrated into the calculation of the channel matrix.

5 Differential Summation Algorithm for Modified IRS Channel Gain

5.1 Algorithm in Details

This section introduces a differential summation algorithm applicable for modified IRS channel gain, thereby supporting the subsequent simulation analysis of performance variations caused by alignment errors. For simplicity, unless otherwise specified, bold capital letters (e.g., $\mathbf{A}$) denote the three-dimensional (3D) coordinates of a point A. A vector is represented by two bold capital letters (e.g., $\mathbf{AB}$ represents a vector from point A to point B), and $\widehat{\mathbf{AB}}$ is its unit vector of $\mathbf{AB}$. $\mathbf{A}(a)$ or $\mathbf{AB}(a)$ represents the a-th element of a coordinate or vector.

According to Section 4, the core of the algorithm is to calculate the reflection points on the receiver plane for lights passing through the center point and the four vertices of any sub-IRS. Since all points on the IRS rotate synchronously and exhibit consistent reflection characteristics, the calculation method for the reflection points is universally applicable. Based on this feature, a single point on the IRS is taken as an example for detailed illustration. Following the setup in Figure 1, to simplify the tracking of individual rays, the coordinate mapping follows a clear geometric process. The IRS element's stationary geometry is first defined in a localized coordinate system. Synchronized 3D rotation matrices are then applied to model tracking deviations, and finally, the rotated coordinates are mapped back into the global reference frame to locate the exact reflection spot on the receiving plane. Specifically, a 3D local coordinate system is established with its origin at the IRS center point (e.g., $\mathbf{M}_{\mathrm{L}} = [0,0,0]^T$). Any point on the IRS in this local coordinate system is denoted as $\mathbf{M}_{\mathrm{G}} = [0, y_{\mathrm{L}}, z_{\mathrm{L}}]^T$, where y_{L} and z_{L} represent arbitrary real numbers. Furthermore, a 3D global coordinate system is established with the origin at point O. Let $\mathbf{P}$, $\mathbf{M}$, and $\mathbf{R}$ denote the coordinates of the LED point source, an IRS center point, and the PD center point in the global coordinate system, respectively.

5.1.1 *Determination of Initial IRS Orientation*

Firstly, the IRS orientation is determined by finding a unit vector $\widehat{\mathbf{U}}$ normal to its surface, which can be expressed as:

$$\widehat{\mathbf{U}} = \frac{(\widehat{\mathbf{MP}} + \widehat{\mathbf{MR}})}{\sqrt{2 + 2\widehat{\mathbf{MP}}^{\mathrm{T}}\widehat{\mathbf{MP}}}} \tag{10}$$

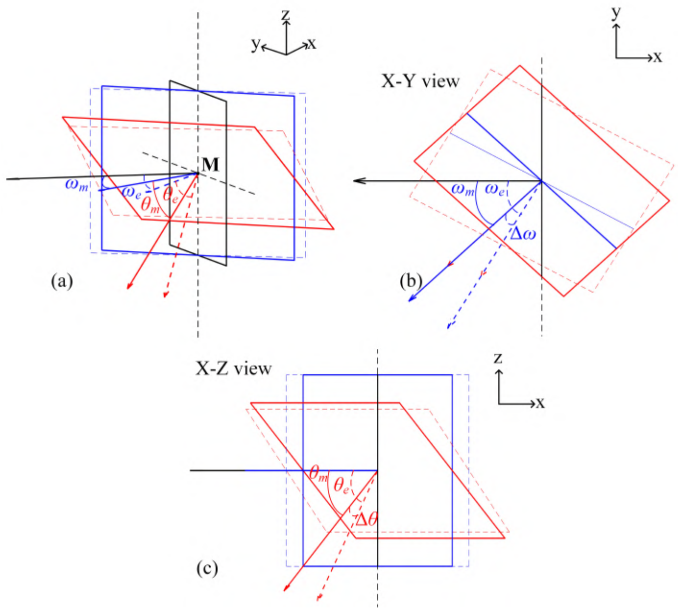

Figure 3. Rotational degrees of freedom of each IRS.

In addition, as shown in Figure 3, IRS orientation is also defined by two orthogonal axes : azimuth angle ω_m (e.g., angle between the projection of the IRS's normal vector onto the x-y plane and the negative x-axis) and polar angle ϑ_m (e.g., angle between the IRS's normal vector and the x-y plane). These two angles defining IRS orientation are expressed in terms of $\widehat{\mathbf{U}}$ as:

$$\widehat{\mathbf{U}} = [-\cos\vartheta_m \cos\omega_m, -\cos\vartheta_m \sin\omega_m, -\sin\vartheta_m]^{\mathrm{T}} \tag{11}$$

Accordingly, the azimuth angle ω_m and polar angle ϑ_m can be calculated by:

$$\begin{aligned} \vartheta_m &= -\sin^{-1}\left(\widehat{\mathbf{U}}(3)\right), \\ \omega_m &= \tan^{-1}\left(\frac{\widehat{\mathbf{U}}(2)}{\widehat{\mathbf{U}}(1)}\right). \end{aligned} \tag{12}$$

5.1.2 Local Coordinate Rotation

Furthermore, the coordinates $\mathbf{M}_{\mathrm{G}}$ of any point on IRS in the local coordinates system after rotation $\tilde{\mathbf{M}}_{\mathrm{G}}$ can be expressed as:

$$\tilde{\mathbf{M}}_{\mathrm{G}} = \boldsymbol{\mathcal{Y}}_{\vartheta_m} \boldsymbol{\mathcal{X}}_{\omega_m} \mathbf{M}_{\mathrm{G}}, \tag{13}$$

where $\boldsymbol{\mathcal{Y}}_{\vartheta_m}$ and $\boldsymbol{\mathcal{X}}_{\omega_m}$ are IRS rotation matrices for ϑ_m and ω_m, respectively, which are expressed as:

$$\boldsymbol{\mathcal{Y}}_{\vartheta_m} = \begin{bmatrix} \cos\vartheta_m & -\sin\vartheta_m & 0 \\ \sin\vartheta_m & \cos\vartheta_m & 0 \\ 0 & 0 & 1 \end{bmatrix} \tag{14}$$

$$\boldsymbol{\mathcal{X}}_{\omega_m} = \begin{bmatrix} \cos\omega_m & 0 & -\sin\omega_m \\ 0 & 1 & 0 \\ \sin\omega_m & 0 & \cos\omega_m \end{bmatrix}. \tag{15}$$

Then, $\tilde{\mathbf{M}}_{\mathrm{G}}$ after rotation in the global coordinates system $\tilde{\mathbf{M}}'_{\mathrm{G}}$ can be represented as:

$$\tilde{\mathbf{M}}'_{\mathrm{G}} = \mathbf{M} + \tilde{\mathbf{M}}_{\mathrm{G}}. \tag{16}$$

5.1.3 Global Projection on The Receiver Plane

The global coordinates $\mathbf{M}_{\mathrm{R}}$ of the reflection from $\tilde{\mathbf{M}}'_{\mathrm{G}}$ on the receiving plane are calculated using the following formula:

$$\mathbf{M}_{\mathrm{R}} = \tilde{\mathbf{M}}'_{\mathrm{G}} + \alpha\widehat{\tilde{\mathbf{M}}'_{\mathrm{G}}\mathbf{M}_{\mathrm{R}}} \tag{17}$$

where α is the normalization coefficient and $\widehat{\tilde{\mathbf{M}}'_{\mathrm{G}}\mathbf{M}_{\mathrm{R}}}$ is the direction vector of reflection, which are as follows:

$$\alpha = \frac{\mathrm{h}_z - \tilde{\mathbf{M}}'_{\mathrm{G}}(3)}{\widehat{\tilde{\mathbf{M}}'_{\mathrm{G}}\mathbf{M}_{\mathrm{R}}}(3)} \tag{18}$$

$$\widehat{\mathbf{M}_{\mathrm{G}}\mathbf{M}_{\mathrm{R}}} = (2\widehat{\mathbf{U}}^{\mathrm{T}}\widehat{\tilde{\mathbf{M}}_{\mathrm{G}}\mathbf{P}})\widehat{\mathbf{U}}^{\mathrm{T}} - \widehat{\mathbf{M}_{\mathrm{G}}\mathbf{P}}, \tag{19}$$

where h_z is the height of the receiving plane. Finally, the complete pseudo-code of the differential summation algorithm for the modified IRS channel model is presented in Algorithm 1. In this algorithm, the IRS is discretized into N sub-IRSs, and the set of their center coordinates in the local coordinate system is represented as $\boldsymbol{\mathcal{M}} = \{\mathbf{M}_{\mathrm{G},1}, \ldots, \mathbf{M}_{\mathrm{G},N}\}$, and the corresponding collection of vertex sets in the local coordinate system is denoted as $\boldsymbol{\mathcal{V}} = \{\mathbf{V}_{\mathrm{L},1}, \ldots, \mathbf{V}_{\mathrm{L},N}\}$, where $\mathbf{V}_{\mathrm{L},n}$ represents the vertex set of the n-th sub-IRS:

$$\mathbf{V}_{\mathrm{L},n} = \{\mathbf{V}_{\mathrm{L},n,1}, \mathbf{V}_{\mathrm{L},n,2}, \mathbf{V}_{\mathrm{L},n,3}, \mathbf{V}_{\mathrm{L},n,4}\}, \mathrm{n} = 1, 2, \ldots, \mathrm{N} \tag{20}$$

The PD is assumed to be a rectangle whose vertices can be obtained through simple geometric relationships, and its vertex set is given by $\boldsymbol{\mathcal{R}} = \{\mathbf{R}_1, \mathbf{R}_2, \mathbf{R}_3, \mathbf{R}_4\}$. On the other hand, Algorithm 1 only considers a single LED-IRS-PD link. In practice, a MIMO-OWC system consists of multiple LEDs, IRSs, and PDs. To scale the algorithm for MIMO scenarios, the orientation of each IRS is determined first. Then, to incorporate all potential interference into the IRS channel gain calculation, the calculation of each sub-channel within the MIMO matrix must repeat Algorithm 1 for M_{IRS} times, where M_{IRS} is the total number of IRS elements.

5.2 Time Complexity Analysis

The classical model is based on the three basic assumptions in Section 3. Under these idealized assumptions, calculating the IRS channel gain for

Algorithm 1: The overall algorithm for the modified IRS channel

Input: $\mathbf{P}$, $\mathbf{M}$, $\mathbf{R}$, $\boldsymbol{\mathcal{M}}$, $\boldsymbol{\mathcal{V}}$, $\boldsymbol{\mathcal{R}}$, ϑ_m, ω_m
Output: $h_{\mathrm{IRS}}^{\mathrm{MP}}$
Calculate the normal vector $\widehat{\mathbf{U}}$ of the IRS after rotation using $\mathbf{P}$, $\mathbf{M}$, $\mathbf{R}$ and Eq.(10).
Calculate ϑ_m and ω_m using Eq.(12).
for $n = 1$ to N **do**
  Calculate the coordinate $\mathbf{M}^{'}_{\mathrm{G,n}}$ using coordinate $\mathbf{M}_{\mathrm{G,n}}$ and Eqs.(13)-(19).
  Calculate the coordinate $\mathbf{V}^{'}_{\mathrm{L,n}}$ using $\mathbf{V}_{\mathrm{L,n}}$ and Eqs.(13)-(19).
  Calculate the irradiance $E_{\mathrm{S},n}$ using $\mathbf{M}_{\mathrm{G},n}$, $\mathbf{M}^{'}_{\mathrm{G},n}$, $\mathbf{P}$ and Eq.(2).
  Calculate the overlapping area A_{S_n} through $\mathbf{V}^{'}_{\mathrm{L},n}$ and $\boldsymbol{\mathcal{R}}$ using the Greiner–Hormann clipping algorithm and polygon triangulation.
  Calculate the photoelectric conversion coefficient $A_{\mathrm{E},n}$ through $\mathbf{M}^{'}_{\mathrm{G},n}$ and $\boldsymbol{\mathcal{R}}$ using (3).
  Calculate the IRS gain $h_{\mathrm{IRS,n}}^{\mathrm{Mod}} = E_{\mathrm{S},n} \times A_{\mathrm{S}_n}$
end for
return $h_{\mathrm{IRS}}^{\mathrm{Mod}} = \sum_{n=1}^{N} h_{\mathrm{IRS,n}}^{\mathrm{Mod}}$

a single IRS takes only dozens of floating-point operations. Consequently, the time complexity of IRS gain for a single IRS can be assumed as $\mathcal{O}(1)$. For a system configured with M_{IRS} elements, the classical model simply repeats this independent calculation M_{IRS} times. As a result, its total time complexity can be denoted as $\mathcal{O}(M_{\mathrm{IRS}})$ for both SISO system and MIMO system.

However, the time complexity of our proposed modified model will be much higher. Specifically, Algorithm 1 calculates the IRS channel gain between a single LED, a single IRS and a single PD. Within this algorithm, each small loop iteration requires dozens of floating-point operations. Since there are N iterations in total, the time complexity for executing Algorithm 1 once is $\mathcal{O}(N)$. Based on this, for a SISO system with M_{IRS} IRS elements, the time complexity becomes $\mathcal{O}(M_{\mathrm{IRS}}N)$. Furthermore, for an $N_t \times N_r$ MIMO system, we must consider the calculation of ICI among different IRS channels. This requires extra N_tN_r loop repetitions. Therefore, the overall time complexity of the proposed modified model is $\mathcal{O}(M_{\mathrm{IRS}}NN_tN_r)$. Although this complexity is much higher than the classical model, this detailed calculation is a necessary and highly valuable trade-off. It allows us to accurately capture the impact of IRS rotation angle error and various IRS sizes.

6 Simulation Results and Analysis

6.1 Simulation Setup

This section systematically evaluates the relative performance of the modified IRS channel model in SISO and MIMO systems under diverse scenarios. All simulations are conducted in a 4 m×4 m×4 m indoor environment, featuring a square IRS array with M_{IRS} elements arranged in an equal number of rows and columns. Each IRS has a side length D, and the array is mounted on the sidewall at the coordinate (4 m, 2 m, 2 m). Note that in all simulations, D and M_{IRS} are adjusted independently without fixing the overall physical area of the IRS array. To ensure practical engineering feasibility during these parameter variations, the overall physical dimensions of the IRS array are strictly bounded such that they neither exceed the boundary of the side wall nor below the height of the receiver plane.

For the SISO-OWC system, a single LED is positioned at the center of the ceiling. In contrast, for the MIMO-OWC system, a 2×2 LED array is utilized, where the individual LEDs are equidistantly mounted on the ceiling, and additional fixed parameters are listed in Table 1. It is noted that the transmitter and receiver parameters, including an LED modulation bandwidth of 20 MHz with a semi-angle of 65°, as well as a standard PD active area of $1\mathrm{cm}^2$ and responsivity of 15 A/W, are selected to be consistent with those adopted in prior indoor OWC experimental and system-level studies [17, 18], ensuring compatibility with standard commercially available off-the-shelf (COTS) optical components. Furthermore, since the performance of the MIMO-OWC system does not depend on a specific sub-channel gain, but rather on the quality of the entire channel matrix, an intuitive metric is needed to evaluate the impact of the IRS on the MIMO system. In this paper, the theoretical BER upper bound is adopted as the evaluation metric to investigate the impact of the IRS. The derived theoretical BER upper bound closely matches the simulated BER results under high SNR conditions, because of the union bound's asymptotic convergence to the exact error probability as the noise variance approaches zero. Therefore, given an appropriate SNR value, the trend of the BER upper bound can truly reflect that of the actual BER. The theoretical BER upper bound of a MIMO-OWC system using maximum likelihood (ML) detection can be expressed

Table 1. Fixed Parameters of IRS-aided OWC system

Parameter	Value
Height of receiving plane, h_z	0.85 m
Position of LED for SISO	(2 m, 2 m, 4 m)
Position of LED for MIMO	(1 m, 1 m, 4 m), (1 m, 3 m, 4 m), (3 m, 1 m, 4 m), (3 m, 3 m, 4 m)
Semi-angle at half power of LED, Ψ	65°
Half-angle FOV of optical lens, Φ	65°
Refractive index q,	1.5
LED spacing	2 m
Modulation bandwidth	20 Mhz
Responsivity of PD, ρ	15 A/W
Active area of PD, A	1 cm^2
Reflectance coefficient of wall, ε	0.8
Reflectance coefficient of IRS, l	0.9

as [19]:

$$\mathrm{BER}_{\mathrm{upper}} \leq \frac{1}{2^R R} \sum_{m^{(1)}=1}^{2^R} \sum_{m^{(2)}=1}^{2^R} \mathrm{d_H}\left(\mathbf{c}_{m^{(1)}}, \mathbf{c}_{m^{(2)}}\right) \times P_e\left(\mathbf{c}_{m^{(1)}} \rightarrow \mathbf{c}_{m^{(2)}}, \gamma_t\right) \tag{21}$$

where R is the spectral efficiency, $\mathrm{d_H}\left(\mathbf{c}_{m^{(1)}}, \mathbf{c}_{m^{(2)}}\right)$ gives the Hamming distance of signal vector between $\mathbf{c}_{m^{(1)}}$ and $\mathbf{c}_{m^{(2)}}$, P_e is the pairwise error probability (PEP), which denotes the probability that the receiver mistakes the transmitted signal vector $\mathbf{c}_{m^{(1)}}$ for $\mathbf{c}_{m^{(2)}}$ for a given transmit SNR γ_t:

$$P_e\left(\mathbf{c}_{m^{(1)}} \rightarrow \mathbf{c}_{m^{(2)}}, \gamma_t\right) \leq \frac{1}{6} e^{-\frac{\|\mathbf{Hc}\|^2}{2}\gamma_t} + \frac{1}{12} e^{-\frac{\|\mathbf{Hc}\|^2}{4}\gamma_t} + \frac{1}{4} e^{-\frac{\|\mathbf{Hc}\|^2}{8}\gamma_t}. \tag{22}$$

If we know the PD receiver position, the LOS and NLOS channels are almost certain, and the change in BER will be completely dependent on the change in the IRS channel, thus demonstrating the impact of IRS error on the BER of the MIMO system.

6.2 Relative Performance of IRS-aided SISO-OWC System

This section compares and evaluates the relative performance of IRS using the modified IRS channel model and the classical IRS channel model in a SISO-OWC system. Subsequently, the variation trends of channel gains for IRS with different numbers and sizes are evaluated under the influence of various degrees of IRS rotation angle errors.

6.2.1 IRS Gain

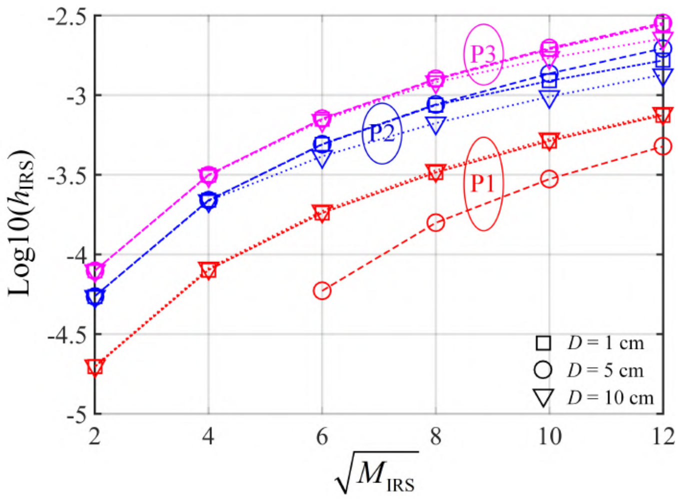

Figure 4. Tendency of ratio of IRS gain to LOS gain at different PD positions and different IRS size with increasing total number of IRSs

Since SISO systems inherently avoid ICI, the classical IRS channel model exhibits high accuracy under precise rotation angles. To validate the accuracy of the modified IRS channel model, a comparative analysis was performed. Figure 4 presents the IRS channel gains across different PD positions and side lengths D for varying M_{IRS}. Specifically, three PD positions are considered: P1 (1.5 m, 2 m, 0.85 m), P2 (2 m, 2 m, 0.85 m), and P3 (2.5 m, 2 m, 0.85 m), which are distributed from far to near relative to the IRS array. Meanwhile, three IRS side lengths are evaluated ($D = 1, 5, 10$ cm). Specifically, $D = 1$ cm complies with the small-reflector assumption but is highly sensitive to IRS rotation angle errors, whereas $D = 5$ and 10 cm violate this assumption yet offer a broader reflection signal coverage. These three IRS sizes are highly appropriate for comprehensively evaluating the impacts of IRS rotation angle errors and the resulting ICI. The lines denote the modified IRS channel model, while the symbols represent the classical IRS model. The results reveal strong consistency between the two models across varying positions, IRS counts, and sizes, thereby validating the practical precision of the modified model.

6.2.2 IRS Gain Impact by IRS Rotation Angle Error

In this section, we will discuss the effect of IRS rotation angle error on IRS gain. Specifically, we define the error

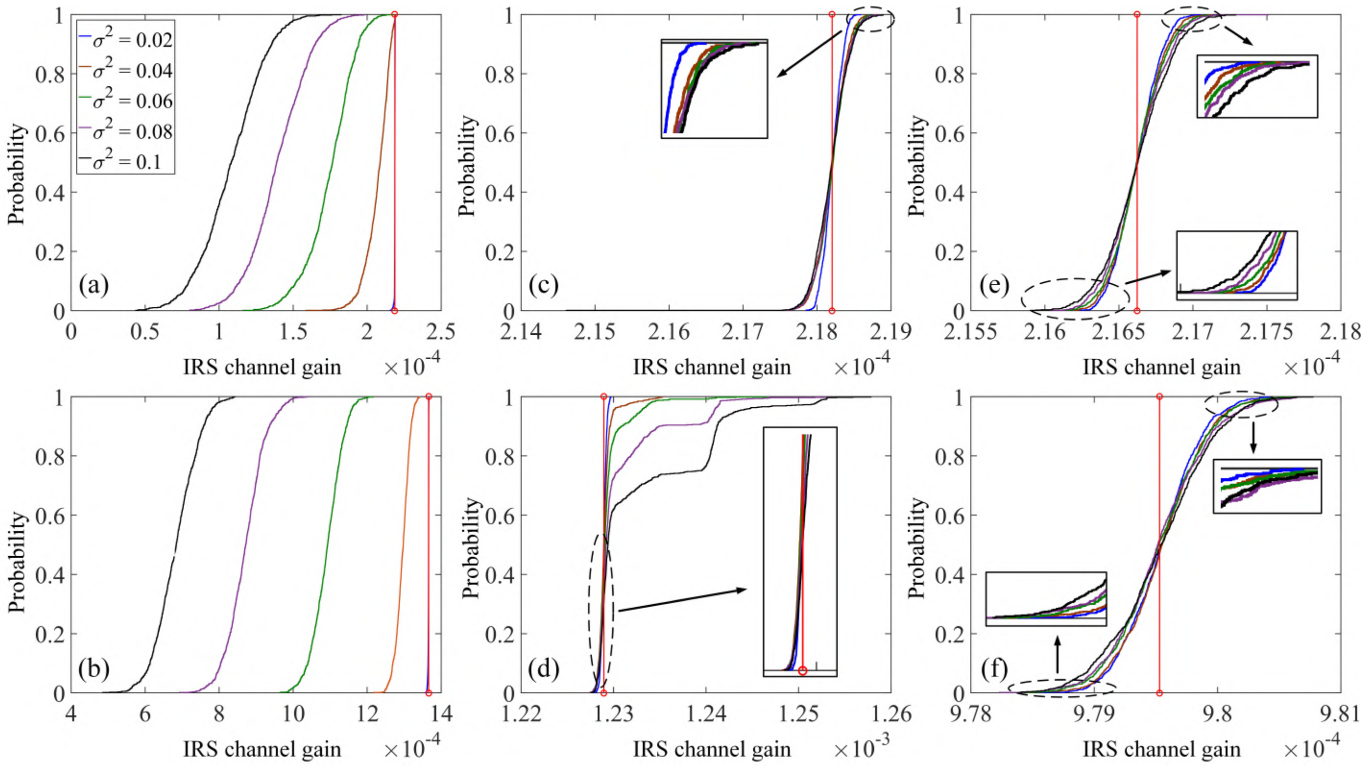

Figure 5. The empirical CDF of the IRS channel gain in the SISO system with different σ^2 at P2. (a) $M_{\mathrm{IRS}} = 16$, $D = 1$ cm, (b) $M_{\mathrm{IRS}} = 100$, $D = 1$ cm, (c) $M_{\mathrm{IRS}} = 16$, $D = 5$ cm, (d) $M_{\mathrm{IRS}} = 100$, $D = 5$ cm. (e) $M_{\mathrm{IRS}} = 16$, $D = 10$ cm, (f) $M_{\mathrm{IRS}} = 100$, $D = 10$ cm.

angles $\Delta\vartheta$ and $\Delta\omega$ (in degrees) as two independent and identically distributed (i.i.d.) Gaussian random variables, i.e., $\Delta\vartheta, \Delta\omega \sim$ i.i.d. $\mathcal{N}\left(0, \sigma^2\right)$. Then, the azimuth angle and polar angle with errors can be expressed as:

$$\begin{aligned} \vartheta_e &= \vartheta_m + \Delta\vartheta \\ \omega_e &= \omega_m + \Delta\omega \end{aligned} \tag{23}$$

Furthermore, the error variance is swept from 0.02 to 0.1 to cover the IRS rotation angle error from small to large values. Physically, a variance of $\sigma^2 = 0.02$ means that the actual error angle is mostly concentrated within $\pm 0.42^\circ$, representing a high-precision state. As the variance increases to 0.1, the error range expands to approximately $\pm 0.95^\circ$, simulating severe errors. This setting allows us to clearly evaluate how the system performance degrades as the IRS rotation angle error grows. For each variance, 1000 independent random trials are performed, and the collected IRS gains are utilized to construct an empirical cumulative distribution function (CDF). Figure 5 presents the empirical CDF of the IRS channel gain in the SISO system with different rotation angle errors at P2. The red vertical line represents the baseline of the error-free case. As shown in Figure 5(a), when $M_{\mathrm{IRS}} = 16$ and $D = 1$ cm, the IRS channel gain has almost no change and stays the same as the baseline when $\sigma^2 = 0.02$. However, as σ^2 increases, the fluctuation range of the IRS channel gain becomes large, and it moves toward smaller values compared to the baseline, where the minimum value is only about one-quarter of the baseline. This phenomenon happens because a small D makes the effective signal coverage area too small, so the signal easily misses the PD, leading to a high probability of reduced IRS channel gain. Conversely, when $M_{\mathrm{IRS}} = 16$ with $D = 5$ cm and $D = 10$ cm, as shown in Figures 5(c) and 5(e), the fluctuation range of the IRS channel gain is relatively small under different σ^2 values, with only about a 5% fluctuation compared to the baseline gain. This is because a larger IRS provides a larger effective signal coverage area, which is big enough to fully cover the PD even with angle errors. However, slight changes in the irradiance on the PD surface also cause small fluctuations in the IRS channel gain. Figures 5(b), 5(d) and 5(f) show the cases for $M_{\mathrm{IRS}} = 100$, which have similar trends to $M_{\mathrm{IRS}} = 16$. From the view of the channel gain variation range, the IRS rotation angle error has a significant impact on the IRS channel gain when $D = 1$ cm, but has slight impact when $D = 5$ cm and $D = 10$ cm. Therefore, it can be seen that in a SISO-OWC system, a larger IRS size can provide a larger effective signal coverage area, better reducing the impact of IRS rotation angle errors.

6.3 Relative Performance of IRS-aided MIMO-OWC System

To comprehensively evaluate the relative performance of the IRS using the modified IRS channel model and the classical IRS channel model in a MIMO-OWC system, a 4-PAM-based 4×4 MIMO-OWC system is adopted in this section, and the evaluation takes into account the impacts of LOS, NLOS, and IRS channels. In typical indoor MIMO-OWC systems, the channel gain might be different for different LED/PD pairs due to the specific distance and emission/incident angle of each LED/PD pair. Hence, the received SNRs corresponding to different LED/PD pairs may differ [6]. To provide a fair and intuitive baseline for the whole system, we use the transmitted SNR of each LED as the common parameter for performance evaluation. Specifically, transmitted SNR is defined as the ratio of the transmitted electrical signal power P_s to the additive noise power P_n, i.e., P_s/P_n.

6.3.1 Theoretical BER Upper Bound

This section evaluates the theoretical BER upper bound of the IRS within the MIMO-OWC system, considering the same three PD array positions as in the aforementioned SISO-OWC system. Figure 6 illustrates the theoretical BER upper bound versus the transmit SNR for the MIMO-OWC system at P2 with no IRS rotation angle errors. Here, the IRS array are assumed to be equally allocated to the four sub-channels corresponding to the diagonal entries of the channel matrix, and the impact of the PD spacing d is additionally taken into account. The BER upper bound curves derived from both channel models are provided for comparison. As shown in Figure 6(a), when $d = 10$ cm and $D = 1$ cm, the BER upper bound curves of the two channel models perfectly overlap. This indicates that the effective signal coverage of each IRS successfully encompasses its designated PD without causing crosstalk to other PDs, thereby yielding matched IRS channel gains between the two models. When the PD spacing is shortened to $d = 5$ cm, Figure 6(b) shows that the BER upper bound curves calculated by the two models also stay the same. When the IRS side length is increased to $D = 5$ cm for the case of $d = 10$ cm, as shown in Figure 6(c), the BER upper bound curves of the two channel models are still very close when $M_{\text{IRS}} = 4$ and $M_{\text{IRS}} = 16$. However, as M_{IRS} continues to increase, the BER curves of the two channel models start to show differences, and the modified IRS channel model shows a worse theoretical BER. For example, when $M_{\text{IRS}} = 36$, the IRS channel matrices calculated in the two channel models are given as follows:

$$\mathbf{H}_{\text{Mod}} \approx 10^{-3} \begin{pmatrix} 0.2759 & 0.0941 & 0.0912 & 0.0941 \\ 0.0941 & 0.1641 & 0.0942 & 0.0912 \\ 0.0912 & 0.0942 & 0.1641 & 0.0941 \\ 0.0941 & 0.0912 & 0.0941 & 0.2759 \end{pmatrix}$$

$$\mathbf{H}_{\text{Cla}} \approx 10^{-3} \begin{pmatrix} 0.1787 & 0 & 0 & 0 \\ 0 & 0.06689 & 0 & 0 \\ 0 & 0 & 0.06689 & 0 \\ 0 & 0 & 0 & 0.1787 \end{pmatrix}$$

From the two channel matrices, it can be seen that because the larger IRS size makes the effective signal coverage area of some IRS elements cover multiple PDs, it causes interference among the sub-channels in the modified IRS channel matrix, which makes the system BER performance worse. This shows the limitation of the classical IRS channel model in MIMO systems, as it cannot calculate the effect of this interference. When the PD spacing is reduced to $d = 5$ cm, as shown in Figure 6(d), the theoretical BER upper bound curves calculated by the two channel models are different. This is because the closer PD spacing leads to more serious ICI. Finally, when the IRS side length is increased to $D = 10$ cm, for both $d = 10$ cm and $d = 5$ cm, as shown in Figures 6(e) and 6(f), the theoretical BER upper bound curves calculated by the two channel models are also different, and the BER curves of the modified IRS channel model is much worse than that of the classical IRS channel model. In conclusion, from Figure 6, under zero IRS rotation angle errors in MIMO-OWC systems, the classical IRS channel model is relatively accurate when the IRS size is relatively small. However, when the IRS size increases, the effective signal coverage area of the IRS may cover multiple PDs, causing ICI and increasing the BER. This situation becomes even worse when the PD spacing becomes smaller. At this time, the classical IRS channel model is no longer accurate.

6.3.2 Theoretical BER Upper Bound Impact by IRS Rotation Angle Error

Finally, Figure 7 shows the empirical CDF of the theoretical BER upper bound for the MIMO-OWC system at P2 with $M_{\text{IRS}} = 16$ under different IRS parameters. Here, the base-10 logarithm of the theoretical BER is used to clearly show the trend. Specific transmit SNR values are chosen for different PD array positions to keep the BER variations within

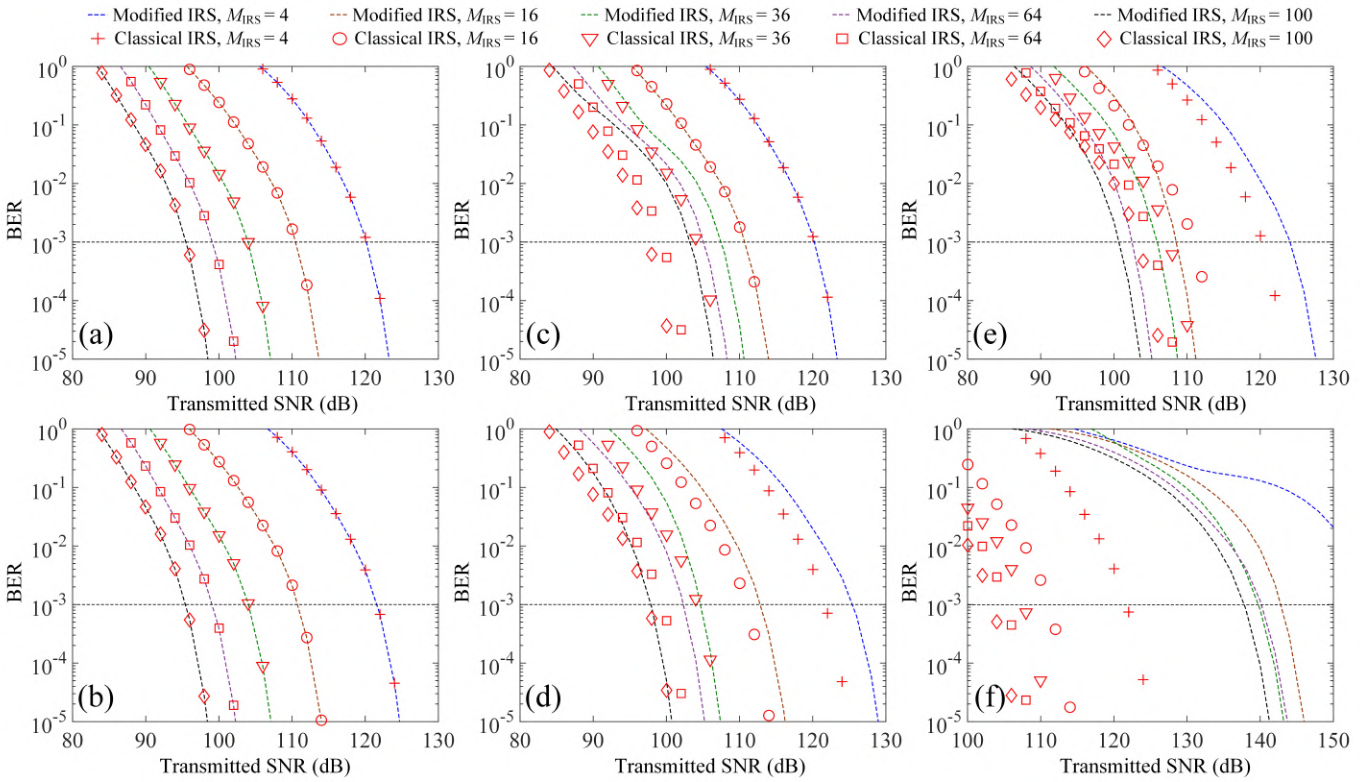

Figure 6. The theoretical upper bound on the BER in MIMO system at P2.
(a) $d = 10$ cm, $D = 1$ cm, (b) $d = 5$ cm, $D = 1$ cm, (c) $d = 10$ cm, $D = 5$ cm,
(d) $d = 5$ cm, $D = 5$ cm. (e) $d = 10$ cm, $D = 10$ cm, (f) $d = 5$ cm, $D = 10$ cm.

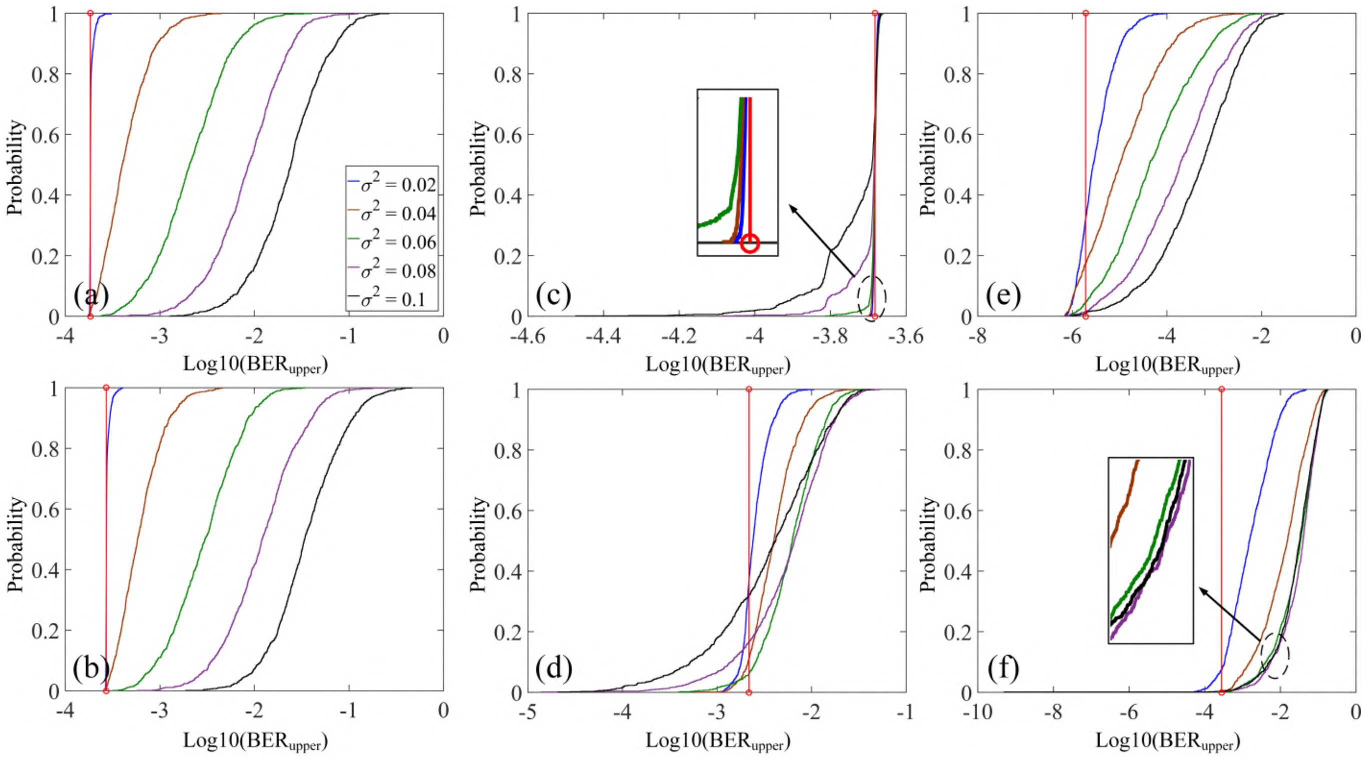

Figure 7. The empirical CDF of the theoretical upper bound on the BER of 16 mirrors in the MIMO system with different σ^2 at P2. (a)-(e) 112 dB transmitted SNR, (f) 144 dB transmitted SNR

a meaningful range. Figure 7(a) shows the BER CDF for $d = 10$ cm and $D = 1$ cm. Under a very small error like $\sigma^2 = 0.02$, the BER variation range is very small compared to the baseline. However, as σ^2 increases, the BER variation range becomes larger, and the BER distribution tends to shift toward higher values compared to the baseline. When the PD spacing is shortened to $d = 5$ cm, as shown in Figure 7(b), the trend of BER CDF is similar to Figure 7(a). As σ^2 increases, the BER variation range increases significantly, and the BER distribution shifts toward higher values. Figure 7(c) shows the BER CDF for $d = 10$ cm and $D = 5$ cm. For all σ^2 cases, the BER change is not significant, and its distribution shifts toward lower values compared to the baseline. When the PD spacing is shortened to $d = 5$ cm, as shown in Figure 7(d), the BER variation range expands and stays around the baseline as σ^2 increases. Figure 7(e) shows the BER CDF for $d = 10$ cm and $D = 10$ cm. It can be seen that as σ^2 increases, the BER distribution also shifts toward higher values compared to the baseline. When the PD spacing is shortened to $d = 5$ cm, as shown in Figure 7(f), the BER variation range expands and shifts toward higher values as σ^2 increases. However, when σ^2 is above 0.06, the BER distribution no longer changes significantly. From the results in Figure 7, it can be seen that the IRS rotation angle error has a significant impact on the MIMO-OWC system. For small IRS sizes, such as in Figures 7(a) and 7(b), the IRS rotation angle error has a big negative impact on the BER performance. This is because the IRS rotation angle error makes the effective signal area miss the assigned PD, causing IRS power loss, or point to the wrong PD, causing ICI. For a larger IRS size, although it can improve the performance against IRS rotation angle errors in SISO-OWC systems, it may cause the effective signal area to cover multiple PDs in MIMO systems. This also leads to ICI, as shown in Figures 7(c) to 7(f). However, it is worth noting that the IRS rotation error also has a probability to reduce the BER. This is especially clear in Figures 7(c) and 7(d). This happens because the ICI accidentally creates a better channel matrix than the baseline scheme. In conclusion, the IRS in MIMO-OWC systems behaves in a more complex way depending on different parameters, meaning that multiple factors must be considered to ensure its effectiveness.

7 Conclusion

This paper proposes a novel modified IRS channel model and its corresponding channel gain differential summation algorithm. Based on geometric optics and computational geometry, the algorithm accurately calculates the IRS channel gain from any LED to different PDs via IRS reflection, thereby considering potential ICI. This model accounts for IRS rotation angle errors and overcomes the traditional small reflector limitation, making it applicable to any IRS size. To validate its accuracy and system impact, comprehensive simulations are performed in typical SISO-OWC and 4×4 MIMO-OWC systems. In the SISO-OWC system, the calculated channel gains match those of the classical model, validating the algorithm's accuracy. Moreover, results show that a larger IRS size effectively mitigates the impact of IRS rotation errors. In the MIMO-OWC system, the IRS introduces no significant interference when the small-reflector is applied and the PD spacing is large. However, as the IRS size scales up, ICI becomes severe, degrading the system BER upper bound. Compared with the classical model, the modified model more realistically reflects the impacts of IRS size and PD spacing. Finally, simulation results reveal that the impact of IRS rotation angle errors on the BER upper bound exhibits randomness under different configurations, implying that IRS designs must be tailored to the concrete conditions of the MIMO-OWC system. These simulation results show that practical hardware implementation faces major challenges, such as high-precision beam-tracking and micro-mirror control. Consequently, overcoming these hardware limitations remains an important direction for future research.

Data Availability Statement

Data will be made available on request.

Funding

This work was supported in part by the National Natural Science Foundation of China under Grant 62271091 and Grant 62501088; in part by the Fundamental Research Funds for the Central Universities under Grant 2024CDJXY020.

Conflicts of Interest

Chen Chen served as an Editorial Board Member of the *Optical Wireless Communication* at the time of manuscript submission. To ensure the integrity of the peer-review process, Chen Chen was not involved in the editorial handling, peer review, or decision-making process for this manuscript, which was handled independently by another editor. The remaining authors declare no conflicts of interest.

AI Use Statement

The authors declare that no generative AI was used in the preparation of this manuscript.

Ethical Approval and Consent to Participate

Not applicable.

References

[1] Katz, M., & Ahmed, I. (2020). Opportunities and challenges for visible light communications in 6G. *2020 2nd 6G wireless summit (6G SUMMIT)*, 1-5. [CrossRef]

[2] Komine, T., & Nakagawa, M. (2004). Fundamental analysis for visible-light communication system using LED lights. *IEEE transactions on Consumer Electronics, 50*(1), 100-107. [CrossRef]

[3] Wu, Q., & Zhang, R. (2019). Intelligent reflecting surface enhanced wireless network via joint active and passive beamforming. *IEEE transactions on wireless communications, 18*(11), 5394-5409. [CrossRef]

[4] Abdelhady, A. M., Salem, A. K. S., Amin, O., Shihada, B., & Alouini, M. S. (2020). Visible light communications via intelligent reflecting surfaces: Metasurfaces vs mirror arrays. *IEEE Open Journal of the Communications Society, 2*, 1-20. [CrossRef]

[5] Zhao, Y., Zeng, Z., Cao, H., & Chen, C. (2025). Enhanced transmitter designs for indoor MIMO-VLC systems. *Optics Communications, 575*, 131279. [CrossRef]

[6] Chen, C., Zhong, X., Fu, S., Jian, X., Liu, M., Yang, H., ... & Fu, H. Y. (2021). OFDM-based generalized optical MIMO. *Journal of Lightwave Technology, 39*(19), 6063-6075. [CrossRef]

[7] Zhong, X., Chen, C., Wen, W., Liu, M., Fu, H. Y., & Haas, H. (2024). Optimization of surface configuration in IRS-aided MIMO-VLC: A BER minimization approach. *IEEE Photonics Journal, 16*(3), 1-12. [CrossRef]

[8] Kahn, J. M., & Barry, J. R. (1997). Wireless infrared communications. *Proceedings of the IEEE, 85*(2), 265-298. [CrossRef]

[9] Abdelhady, A. M., Amin, O., Salem, A. K. S., Alouini, M. S., & Shihada, B. (2022). Channel characterization of IRS-based visible light communication systems. *IEEE Transactions on Communications, 70*(3), 1913-1926. [CrossRef]

[10] Sun, S., Wang, T., Yang, F., Song, J., & Han, Z. (2021). Intelligent reflecting surface-aided visible light communications: Potentials and challenges. *IEEE Vehicular Technology Magazine, 17*(1), 47-56. [CrossRef]

[11] Najafi, M., Schmauss, B., & Schober, R. (2021). Intelligent reflecting surfaces for free space optical communication systems. *IEEE transactions on communications, 69*(9), 6134-6151. [CrossRef]

[12] Wu, Q., Zhang, J., Zhang, Y., Xin, G., & Guo, J. (2022). Configuring reconfigurable intelligent surface for parallel MIMO visible light communications with asymptotic capacity maximization. *Applied Sciences, 13*(1), 563. [CrossRef]

[13] Sun, S., Mei, W., Yang, F., An, N., Song, J., & Zhang, R. (2023). Optical intelligent reflecting surface assisted MIMO VLC: Channel modeling and capacity characterization. *IEEE Transactions on Wireless Communications, 23*(3), 2125-2139. [CrossRef]

[14] Sun, S., Yang, F., Song, J., & Zhang, R. (2023). Intelligent reflecting surface for MIMO VLC: Joint design of surface configuration and transceiver signal processing. *IEEE Transactions on Wireless Communications, 22*(9), 5785-5799. [CrossRef]

[15] Greiner, G., & Hormann, K. (1998). Efficient clipping of arbitrary polygons. *ACM Transactions on Graphics (TOG), 17*(2), 71-83. [CrossRef]

[16] Toussaint, G. T. (1984). A new linear algorithm for triangulating monotone polygons. *Pattern Recognition Letters, 2*(3), 155-158. [CrossRef]

[17] Chen, C., Zhong, W. D., & Wu, D. (2016, June). Indoor OFDM visible light communications employing adaptive digital pre-frequency domain equalization. In *2016 Conference on Lasers and Electro-Optics (CLEO)* (pp. 1-2). IEEE. https://ieeexplore.ieee.org/abstract/document/7787995

[18] Chen, C., Zhong, W. D., & Wu, D. (2017). On the coverage of multiple-input multiple-output visible light communications. *Journal of Optical Communications and Networking, 9*(9), D31-D41. [CrossRef]

[19] Chiani, M., Dardari, D., & Simon, M. K. (2003). New exponential bounds and approximations for the computation of error probability in fading channels. *IEEE Transactions on Wireless Communications, 2*(4), 840-845. [CrossRef]